JOURNAL OF GEOPHYSICAL RESEARCH, VOL. 105, NO. A3, PAGES 5081–5092, MARCH 1, 2000

Detection of coronal mass ejection associated shock waves in the outer corona

N. R. Sheeley Jr., W. N. Hakala,[1] and Y.-M. Wang

E. O. Hulburt Center for Space Research, Naval Research Laboratory, Washington, D. C.

Abstract. White light coronal images from the Large-Angle Spectrometric Coronagraph (LASCO) on the Solar and Heliospheric Observatory (SOHO) spacecraft show disturbances propagating away from high-speed coronal mass ejections (CMEs). The disturbances are faintly visible ahead of the ejected material at the noses of the CMEs but are strongly visible along the flanks and rear ends, where they produce kinks in the streamers and other raylike features that extend in all directions from the Sun at this phase of the sunspot cycle. The kinks decelerate as they move radially outward along the rays, apparently indicating the slowing of the entire wave front as it passes by. For a fast CME seen head on (or tail on) the deceleration occurs at virtually all position angles around the occulting disk. However, for a CME seen obliquely the speed varies strongly with position angle, being fast and uniform near the nose but slower and decelerating at the sides and rear where the deflected rays are more inclined from the sky plane and farther from the Sun. The initial speeds ($\gtrsim$800–1400 km/s) are faster than the nominal MHD speed ($\sim$600 km/s) at these heights, implying that these disturbances are shock waves, made visible like "amber waves of grain" [*Bates*, 1895] in the field of coronal rays around the Sun.

1. Introduction

The idea that shock waves originate at the Sun is not new. In a symposium held in July 1953, *Gold* [1955] argued that the sudden commencements of geomagnetic storms are too rapid to be caused by dispersive particle streams from the Sun and are more likely caused by shock waves with relatively sharp wave fronts. In the same session, *Liepmann* [1955] immediately challenged this interpretation, noting that such sharp wave fronts would be 100 times smaller than the mean free path of the particles in the interplanetary gas. As *Parker* [1963] later pointed out, Gold realized that the shock thickness is determined by the radius of gyration of the particles in the magnetic field, rather than by their classical mean free path, and the concept of "collisionless" shocks was born.

Meanwhile, in Australia, radio scientists were finding observational support for the solar origin of such shock waves. J. P. Wild and his colleagues observed type II metric radio bursts moving outward from solar flares at speeds of the order of 500 km/s or more [*Wild et al*., 1953] and soon suggested that these type II bursts were caused by shock waves moving outward through the corona [*Wild et al*., 1963; *Wild and Smerd*, 1972].

As spacecraft began to explore the solar system, the evidence became overwhelming. Shocks were sampled in situ by the Mariner 2 plasma detector [*Sonett et al*., 1964], and type II bursts were tracked continuously from the Sun to Earth with low-frequency radio instruments on ISEE 3 [*Cane et al*., 1982]. White light coronagraphs on Earth-orbiting satellites observed fast mass ejections associated with the interplanetary shocks [*Gosling et al*., 1975; *Sheeley et al*., 1985; *Schwenn*, 1986] and type II bursts [*Cane and Stone*, 1984; *Sheeley et al*., 1984; *Robinson et al*., 1986; *Cane et al*., 1987] (see also the review by *Bougeret* [1985]). There seemed little doubt that the coronal mass ejections (CMEs) and flares were somehow responsible for the shocks, by sending material through the ambient medium at super-Alfvenic speeds or by releasing energy explosively or both.

However, it was still unclear which coronal features, if any, correspond to the shocks. One possibility was that the shock coincided with the leading edge of the ejected mass. Another possibility was that the shock lies undetected in front of the ejected mass and tapering off to the sides, like the bow shock in front of the Earth's magnetosphere [*Steinholfson*, 1985; *Hundhausen*, 1987]. The invisibility of the shock was supposed to be due to the relatively low sensitivities of the white light coronagraphs of that era. A third possibility was that there may be two shocks: a driven shock ahead of the ejected mass and a blast wave moving through the ejected mass as reported by *Wagner and MacQueen* [1983].

Hundhausen [1987] considered the possibility that shocks might be responsible for the streamer deflections that frequently accompany CMEs. Noting that only a small fraction of observed CMEs move faster than the nominal 600 km/s Alfven speed at 3 R_S, he reasoned that relatively few CMEs would be able to produce the deflections of remote streamers by driving shocks through the corona. In fact, only one event was reported for which a shock interpretation seemed possible [*Sime and Hundhausen*, 1987]. Hundhausen concluded that most of these streamer deflections are caused by compressive magnetoacoustic waves moving out from the sides of CMEs approximately transverse to the nearly radial magnetic field.

In this paper, we present observations of CMEs whose leading edges move outward at speeds in the range 800–1400 km/s, well in excess of the 600 km/s Alfven speed that *Hundhausen* [1987] adopted for 3 R_S. These fast CMEs have "spheres of

[1]Now at Asian and Middle Eastern Languages, University of Virginia, Charlottesville.

Paper number 1999JA000338.

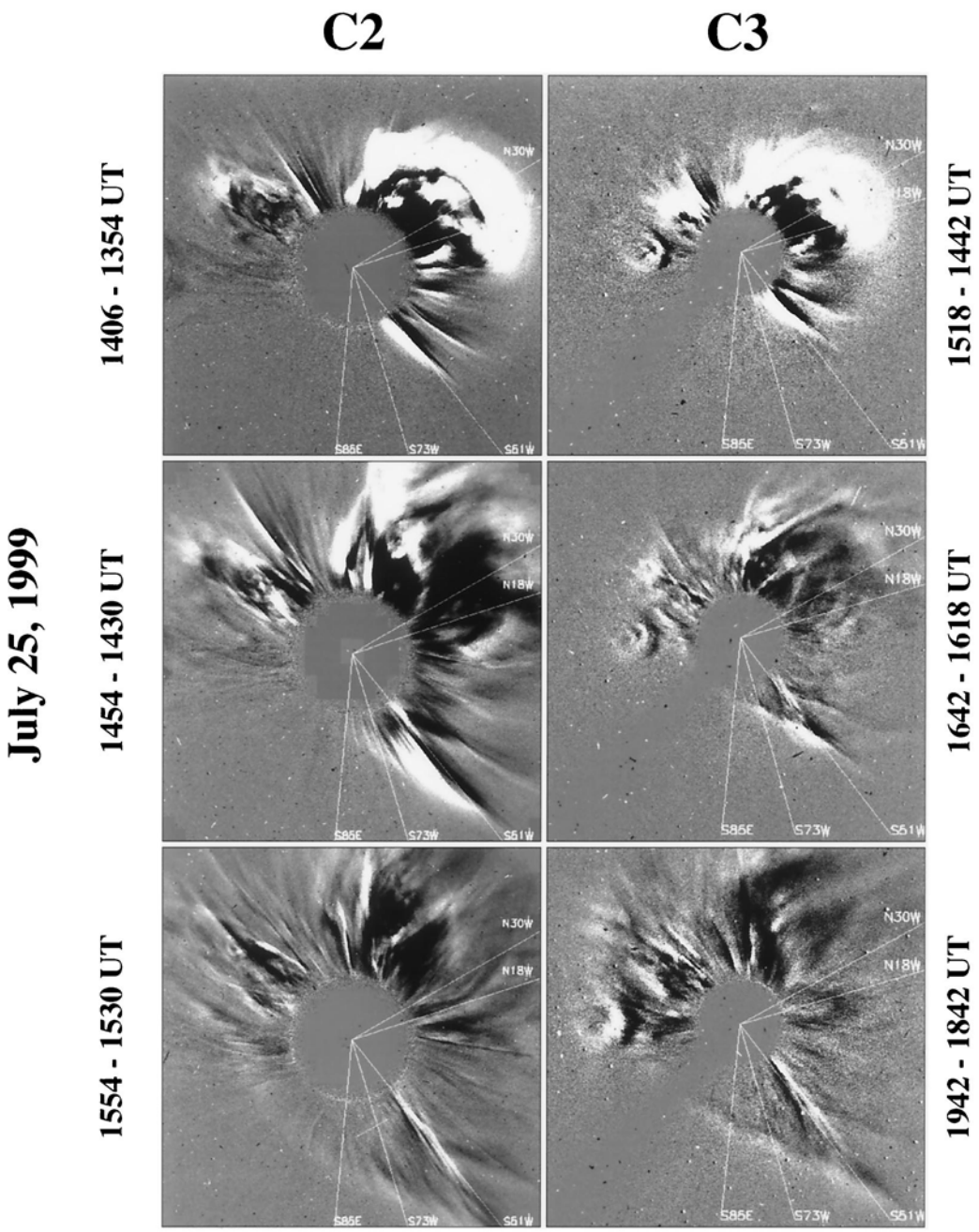

Figure 1a. Running difference images obtained with the (left) C2 and (right) C3 coronagraphs, showing the deflections of numerous rays toward the sides and rear of a large CME on July 25, 1999, and their gradual formation into a large-scale wave front. The deflections are indicated by black-and-white areas whose white components are directed away from the CME. In all figures of this paper the coronal images are arranged so that solar north is up and east is to the left. Likewise, the image scales are given by the sizes of the C2 and C3 occulting disks whose radii are approximately 2.0 R_S and 4.0 R_S, respectively. Thus, in this figure, the cropped C3 field shows an area about 34 R_S on a side, while the C2 field shows a much smaller area only 13 R_S on a side. The radial lines indicate directions for which height/time maps are shown in Figure 1c.

influence" that extend from faint precursors ahead of the ejected mass to the tips of deflected streamers and rays along the sides and toward the rear. Broadside observations of fast CMEs show uniform speeds toward the front but decelerations of the kinks that propagate radially outward along the deflected streamers and rays. Observations, obtained head-on (or tail-on), show decelerations in all directions around the occulting disk. For such fast events we suppose that the observed wave fronts are shocks, slowing down as they push obliquely past the coronal streamers and rays.

2. Observations

We begin with the July 25, 1999, CME, which was ejected into the northwest quadrant and produced a wave of deflected

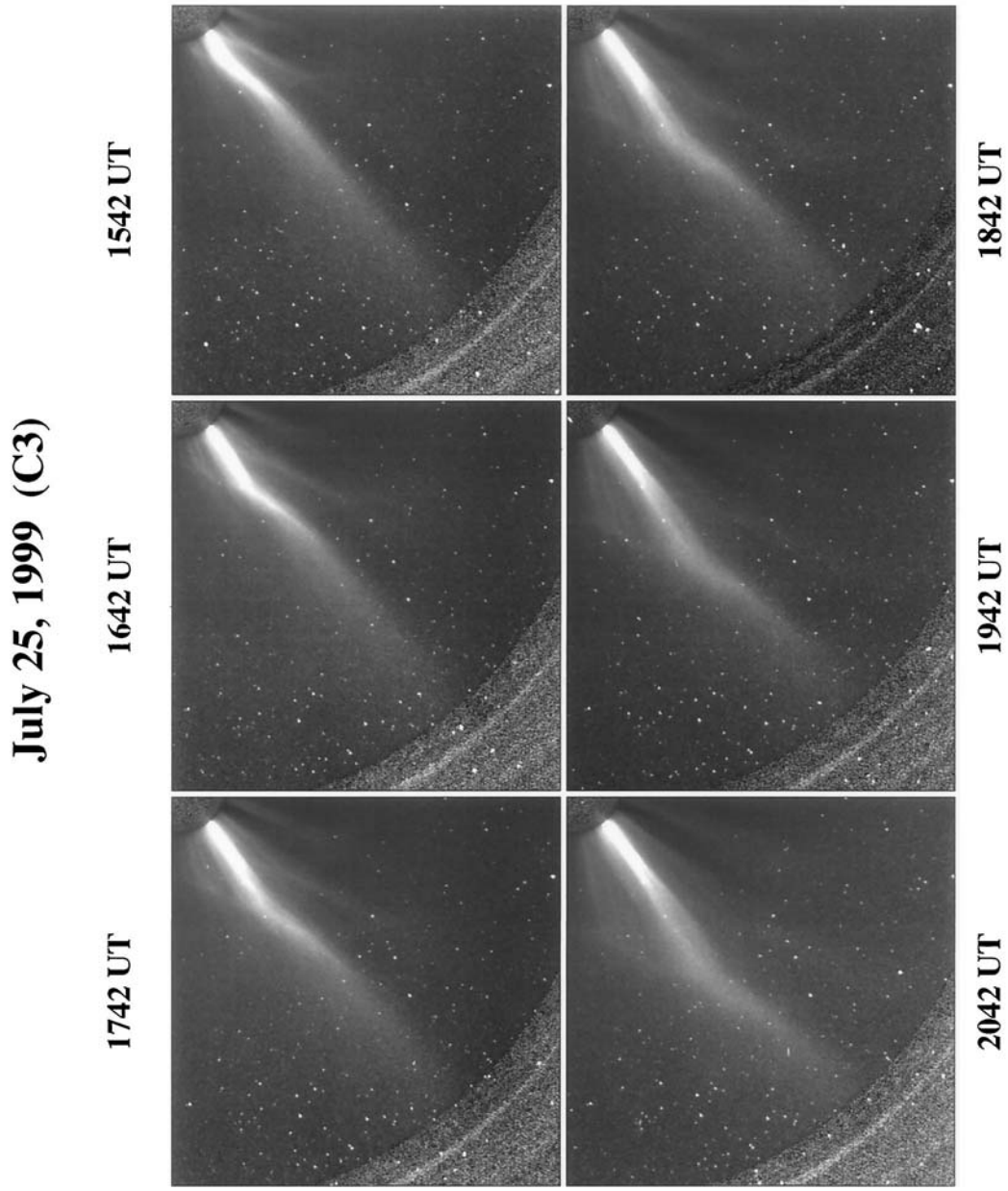

Figure 1b. Coronal intensity images, obtained by dividing each C3 frame by a "monthly minimum" background image, showing that the wave front in Figure 1a is produced by deflection of a coronal streamer and some fainter rays near it on July 25, 1999. Each image shows the southwest portion of the C3 field of view from 4 R_S to 30 R_S.

rays heading southeast. Figure 1a shows the evolution in a sequence of running difference images, obtained by subtracting each image from the next. The outward motion of the CME is accompanied by a progression of deflected rays, first visible along the flanks of the CME and then increasingly farther toward the east. In the top two images the tips of these deflected features seem to be linked to a faint precursor ahead of the much brighter ejected mass.

The individual rays are deflected away from the CME, as indicated by the more distant white portions of the deflected black-and-white features. The progression around the south side of the occulting disk is shown by the succession of deflected rays, including the major one at S51°W. However, the progression around the north side is obscured by a slower moving ejection in the northeast. This loss of visibility is only temporary, and by 1554 UT the two waves are seen to merge into a single arc spanning the southeast quadrant.

The "background-subtracted" images in Figure 1b show that the deflected features are kinks in previously existing bright rays. The brightest of these rays is a coronal streamer, and the fainter ones are probably less visible parts of streamer surfaces deformed and compressed by the disturbance. Although the large-scale wave front moves nonradially across the field, the individual kinks propagate radially outward along their rays. Thus, in Figure 1a the deflection of the streamer at S51°W moves outward along the radial white line drawn at this loca-

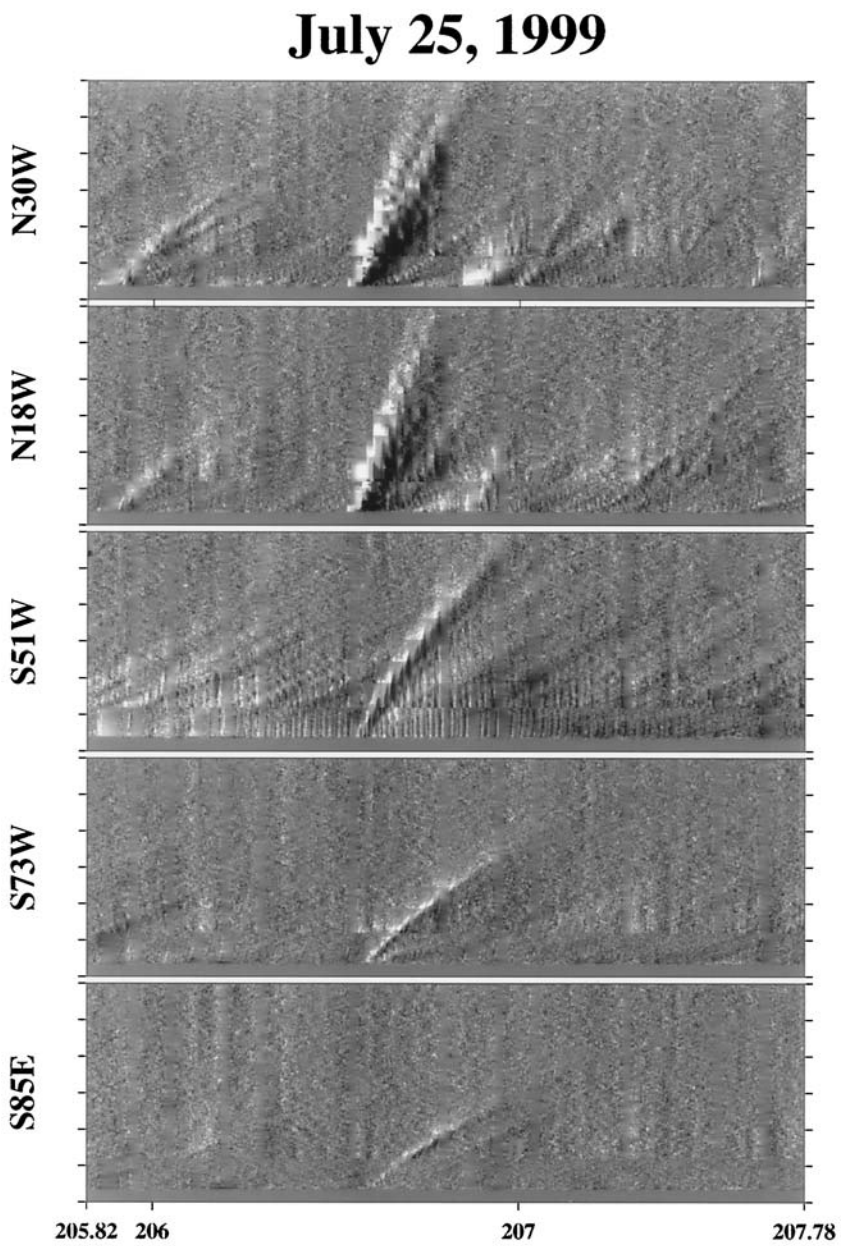

Figure 1c. Height/time maps constructed at the locations indicated in Figure 1a, showing the fast, uniform speed near the nose of the CME and the slower, decelerations along the sides and rear. The horizontal scale indicates time expressed as a day of year, and the vertical scale indicates elongation expressed in solar radii from 0 to 30 R_S.

tion, and the long black-and-white feature forming behind it indicates the repositioning of the streamer after the deflection.

The radial lines on the C2 and C3 images in Figure 1a indicate the angular positions corresponding to the gray-scale height/time maps in Figure 1c. As described previously [*Wang et al*., 1998; *Sheeley*, 1999; *Sheeley et al*., 1999], these maps are constructed by stacking radial strips of individual C2 and C3 difference images side by side, giving a picture of coronal intensity difference as a function of time (day of year along the horizontal axis) and radial position (from 0 to 30 R_S along the vertical axis). In the top two images, the tracks appear steep and straight, indicating that the speed was fast and uniform at the leading edge of the CME at N30°W and N18°W. The corresponding slopes are 1130 and 1230 km/s, respectively. In the bottom three images, the tracks curve slightly downward, indicating that the streamer deflections at S51°W, S73°W, and S85°E decelerate as they move outward. We shall examine these decelerations more closely in Figure 2.

Figure 2a shows six radial paths through the wave front, and Figure 2b shows the corresponding height/time maps. In Figure 2b the height/time tracks all have downward curvatures, indicating decelerations. Also, the slopes of these tracks decrease systematically toward the rear of the event near S75°E, as if the deflected features were farther out of the sky plane there. The nose of the CME, whose projected location was in the vicinity of N18°W–N30°W, probably lay close to the sky plane because the associated event in the lower corona originated close to the limb. In fact, the Fe XII 195 Å images from the Extreme Ultraviolet

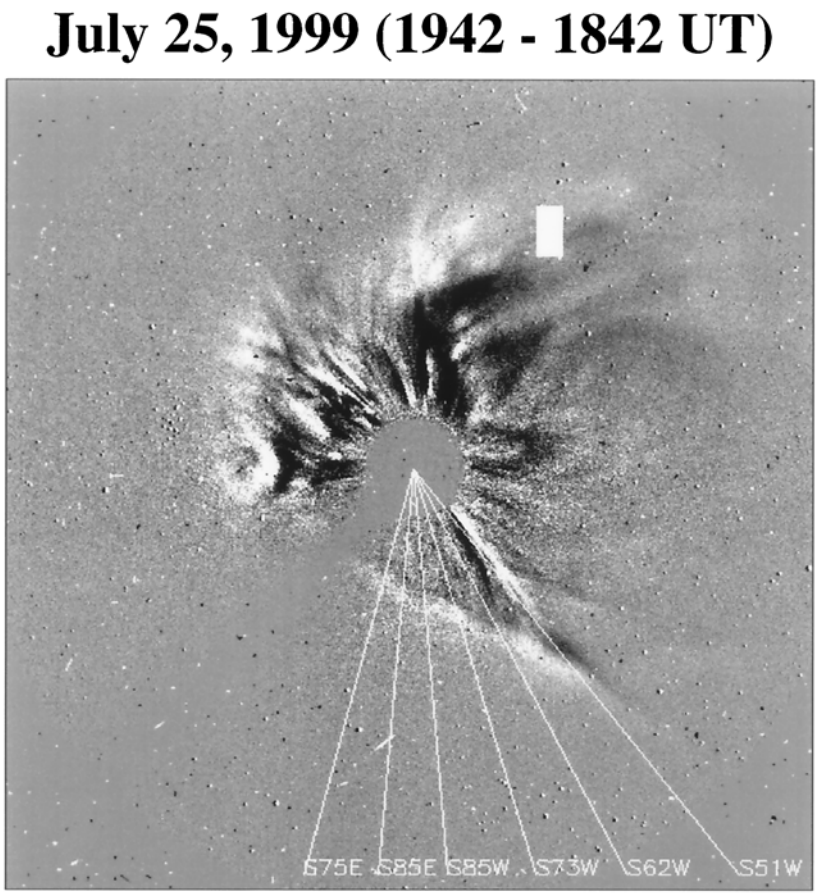

Figure 2a. A C3 difference image on July 25, 1999, showing the southward directed wave front cut by the radial paths for which height/time maps are given in Figure 2b. Whereas the corresponding C3 image in Figure 1a was cropped, this one shows the full field to 30 R_S in the horizontal and vertical directions and to 32 R_S in the corners.

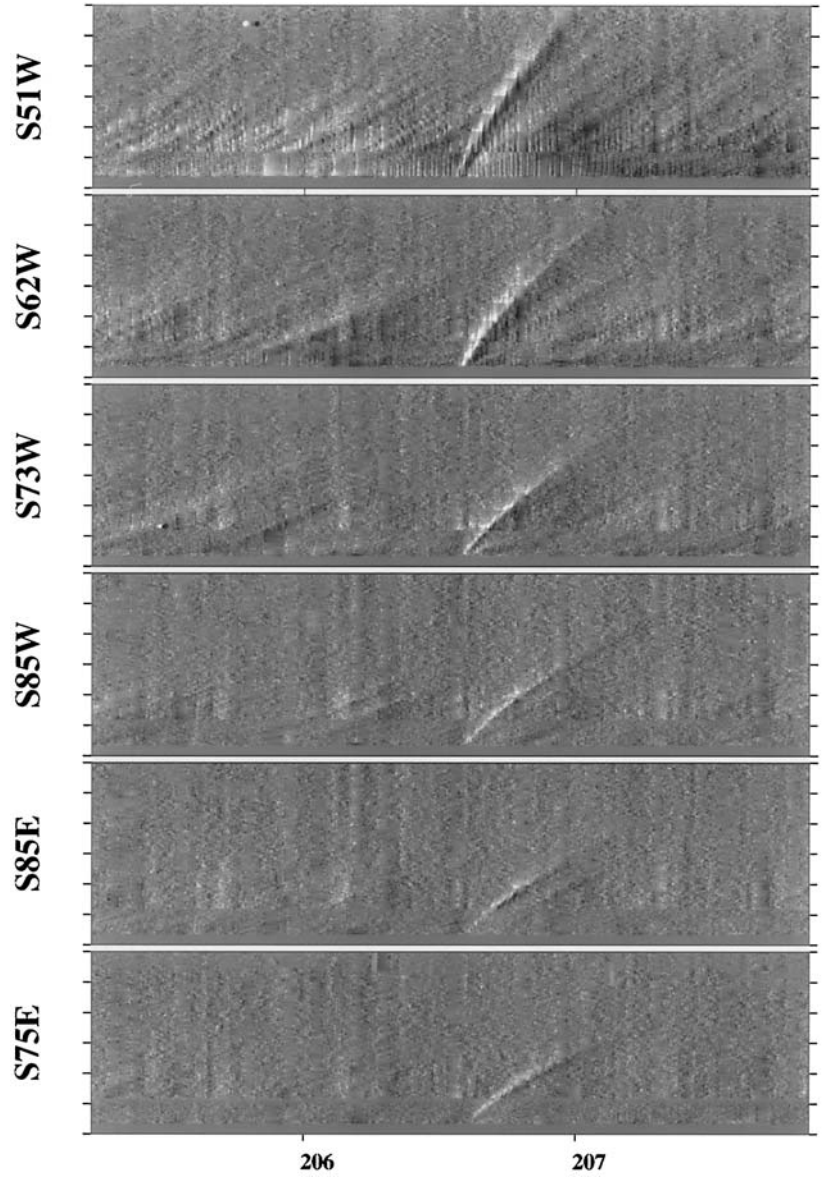

Figure 2b. Height/time maps for the locations indicated in Figure 2a, showing deceleration and the systematic decrease of sky plane speed with angular distance from the nose of the July 24–26, 1999, CME. The horizontal scale indicates time expressed as a day of year, and the vertical scale indicates elongation expressed in solar radii from 0 to 30 R_S. Measurements of these tracks are summarized in Table 1.

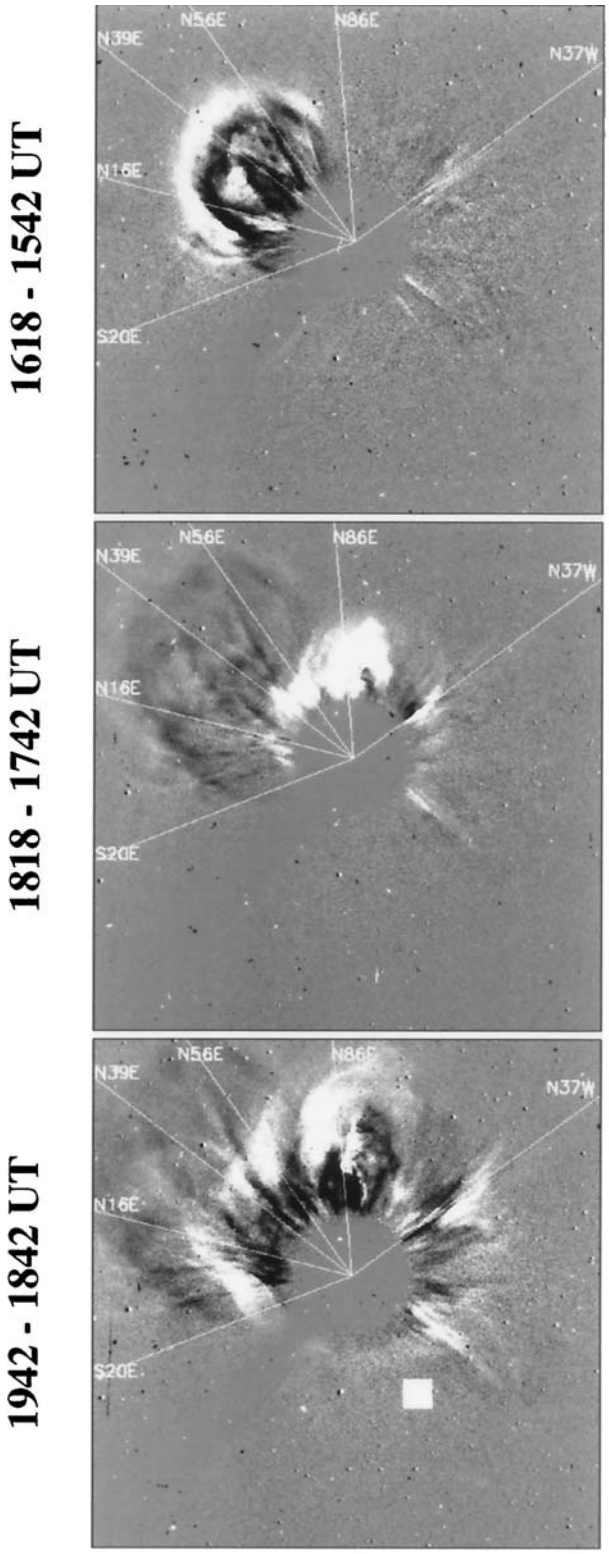

Figure 3a. C3 running difference images, showing a sky plane CME followed by a quasi-halo CME on July 6, 1999. The radial lines indicate paths for which height/time maps are shown in Figure 3b. In each of these C3 images the field of view has been cropped and shows an area of ~37 R_S on a side.

Table 1. Measurements for the CME of July 25, 1999

Position Angle	r_0/R_S	v_0, km/s	v_1, km/s	τ, hours	a_0, m/s^2
S51°W	2.6	780	390	3.4	32
S62°W	2.4	620	280	3.9	24
S73°W	2.3	460	250	3.9	15
S85°W	2.3	430	210	3.3	19
S85°E	2.2	410	190	3.3	18
S75°E	2.6	350	190	3.0	15

Telescope (EIT) on SOHO showed a large eruption with a Moreton-like wave and postflare loops just inside the northwest limb.

We have determined the decelerations by fitting height/time measurements of the downward curving tracks with a function of the form

$$r(t) = r_0 + v_1 t + (1 - e^{-t/\tau})(v_0 - v_1)\tau, \quad (1)$$

where r_0 and v_0 are the position and speed at $t = 0$, and v_1 is the asymptotic speed attained on an e-folding time τ. In this case, the speed changes smoothly from its initial value v_0 toward its smaller asymptotic value v_1 according to

$$v(t) = v_1 + (v_0 - v_1)e^{-t/\tau}, \quad (2)$$

and the acceleration falls exponentially from its initial value $a_0 = (v_0 - v_1)/\tau$ according to

$$a(t) = -a_0 e^{-t/\tau}. \quad (3)$$

These positions, speeds, and accelerations are sky plane components of their radial values. Detailed illustrations of this procedure have been presented previously [*Sheeley et al.*, 1999].

Table 1 summarizes the measurements obtained for the six tracks in Figure 2b. As expected, the starting radii lie just above the C2 occulting disk in the range 2–3 R_S. The initial speeds v_0 decrease systematically from about 780 km/s at S51°W to 350 km/s at S75°E, and the final speeds v_1 decrease from 390 to 190 km/s, all with an accuracy of ~5–10%. The e-folding times τ did not vary systematically with position angle and had an average value of 3.5 hours. However, they were the least reproducible of the fit parameters and had typical accuracies in the range 20–30%. These fit parameters gave decelerations a_0 that decreased systematically from ~32 m/s^2 at S51°W to 15 m/s^2 at S75°E, with accuracies probably in the range 30–50%. Like the speeds, these decelerations are sky plane components of true radial values, which may be 2 or 3 times larger.

These properties of the July 25, 1999, CME are not unusual. Figure 3a compares running difference images of two consecutive CMEs on July 6, 1999. The first CME is visible in the northeast quadrant at 1618 UT. The Fe XII 195 Å EIT images

Table 2. Measurements for the Quasi-Halo CME of July 6, 1999

Position Angle	r_0/R_S	v_0, km/s	v_1, km/s	τ, hours	a_0, m/s^2
N37°W	2.1	1000	480	1.5	97
N86°E	2.1	1420	660	1.5	140
N56°E	2.6	920	420	3.4	40
N39°E	2.7	890	310	4.2	38
N16°E	2.4	880	170	4.8	41
S20°E	2.4	590	250	4.0	20

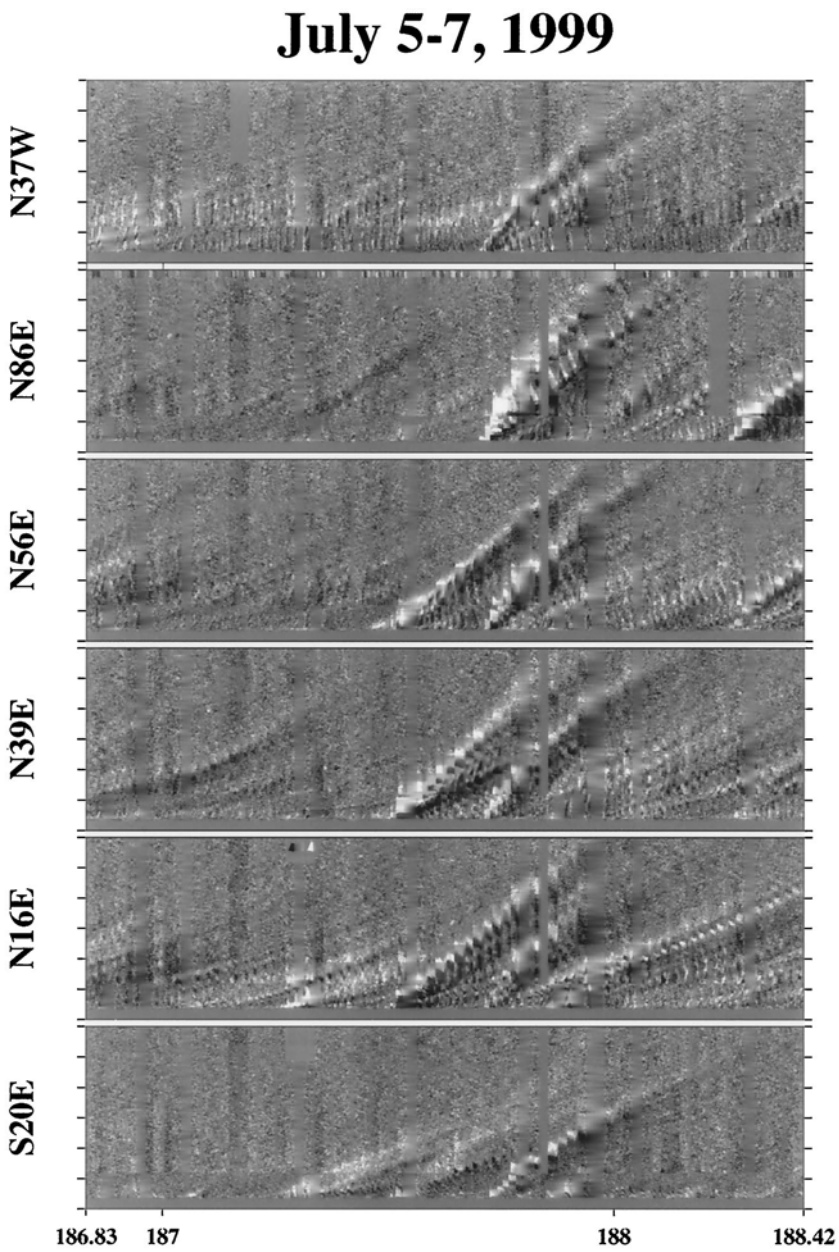

Figure 3b. Height/time maps for the locations indicated in Figure 3a, comparing the relatively straight height/time tracks of the sky plane CME (at N56°E, N39°E, and N16°E) with the downward curving tracks of the quasi-halo CME. The horizontal scale indicates time expressed as a day of year, and the vertical scale indicates elongation expressed in solar radii from 0 to 30 R_S. Measurements of these decelerating tracks are summarized in Table 2.

showed an off-limb depletion followed by postflare loops just inside the east limb, suggesting that this CME was ejected close to the sky plane. As this CME moves outward and fades, a second CME becomes visible, first in the north at 1818 UT and then all around the occulting disk at 1942 UT. The corresponding Fe XII images showed material coming up over the north polar limb around 1700 UT, suggesting that this halo CME originated in the northern hemisphere on the back side of the Sun. In the lower image of Figure 3a, ejected prominence material is visible over the north pole.

Figure 3b shows gray-scale height/time maps obtained along the radial paths indicated by the white lines in Figure 3a. As one can see for N56°E, N39°E, and N16°E, the three cuts through the broadside CME show linear height/time tracks, corresponding to uniform speeds. Linear fits to these tracks give speeds of 490, 560, and 500 km/s, respectively; somewhat slower than most CMEs with constant speeds [cf. *Sheeley et al*., 1999].

By contrast, all of the images show downward curving tracks at the time of the halo CME. Table 2 summarizes the measurements of these tracks. The speeds are initially fast but decrease toward their asymptotic values on a timescale of 1.5–4.8 hours. The starting speed v_0 is largest (1420 km/s) at N86°E, approximately the direction of the ejected material, and decreases systematically toward the rear of the event,

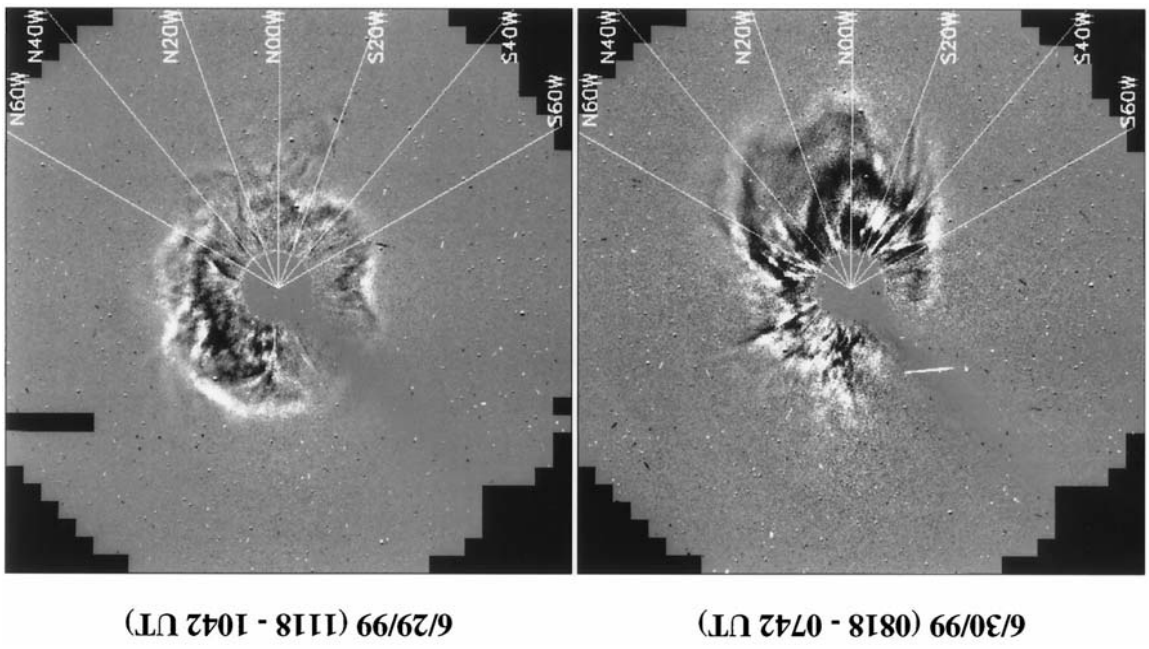

Figure 4a. C3 difference images, comparing a fast CME seen (top) tail-on on June 29, 1999, with (bottom) a quasi-halo CME on June 30, 1999. The radial lines indicate paths for which height/time maps are shown in Figure 4b. In each image the full C3 field of view is shown, extending to 30 R_S in the horizontal and vertical directions and to 32 R_S in the corners.

Figure 4b. Height/time maps for the locations indicated in Figure 4a, comparing the tracks of the June 29 halo CME (whose deceleration is interrupted by a gradually accelerating flow at midlatitude) with the tracks of the June 30 quasi-halo CME (whose sky plane components are fast and uniform at midlatitude but lower and decelerating at high latitude). The horizontal scale indicates time expressed as a day of year, and the vertical scale indicates elongation expressed in solar radii from 0 to 30 R_S.

Table 3. Measurements for the Halo CME of June 29, 1999

Position Angle	r_0/R_S	v_0, km/s	v_1, km/s	τ, hours	a_0, m/s^2
N60°W	2.3	670	330	3.7	25
S33°W	2.5	800	300	2.1	67
S85°W	2.1	500	240	4.6	16
S07°E	2.4	710	360	4.2	23
N32°E	2.5	800	430	2.3	44
N67°E	2.4	680	450	2.2	28
Average	2.4	690	350	3.2	30

reaching 590 km/s at S20°E. The asymptotic speed v_1 shows essentially the same variation, suggesting again that the moving features are farther out of the sky plane toward the rear of the CME. On the other hand, the e-folding times τ are not constant but have relatively small values of 1.5 hours at N37°W and N86°E, compared to 4.8 hours toward the rear of the event. We do not know whether this indicates a real decrease in the amount of radial deceleration toward the tail or whether it is a consequence of the relatively noisy height/time tracks for this event.

Figure 4a compares two CMEs, which again seem to have originated on the back side of the Sun. The June 29, 1999, CME rose up from behind the north polar limb but developed a halo topology by the time of the 1118 UT difference image in the top image. The June 30, 1999, CME was associated with an FeXII 195 Å depletion at the northwest limb around 0412 UT and seems to be a partial halo similar to the second CME on July 6, 1999 (in Figure 3a).

Figure 4b shows the height/time maps corresponding to the radial paths indicated on the images in Figure 4a. These west limb paths include the gap in the June 29 halo and the nose of the June 30 CME. We see that the June 29 event has downward curving tracks toward the northern (N60°W) and southern (S40°W, S60°W) ends of this range, indicating decelerations. Their initial speeds lie in the range 700–1000 km/s and decrease to 350–400 km/s after 1–3 hours. However, in the midlatitude gap the tracks become lost or distorted by the gradually accelerating tracks in the streamer belt, whose asymptotic speeds are ~340–360 km/s. Our movies show that the meandering black track at N40°W on June 29 corresponds to previously ejected slow material that is swept up by the leading edge of the faster halo CME. The tracks of the June 30 CME are like those of the July 6 quasi-halo, being steep and straight near the nose where the speeds lie in the range 800–1050 km/s and curving downward outside this range. At S60°W the tracks of the June 29 and June 30 CMEs are similar, with speeds falling from ~700 to 360 km/s in 2 hours.

Although the June 29, 1999, halo is poorly defined in the northwest, it is very well defined in a variety of directions around the occulting disk. Figure 5a indicates some of these directions, and Figure 5b shows the corresponding height/time maps. Referring to Figure 5b, we can see that the tracks all curve downward, indicating decelerations. We have used equation (1) to fit the measurements of these tracks and have summarized the results in Table 3. Unlike the CMEs of June 30, July 6, and July 25, this well-aligned halo shows no systematic variation of speeds and decelerations with position angle. The initial speeds lie in the range 500–800 km/s and fall toward final speeds of 240–450 km/s in e-folding times of 2.1–4.6 hours. The corresponding initial decelerations lie in the range 16–67 m/s^2, which again are the sky plane components of larger radial decelerations.

On the other hand, some of the azimuthal variations in Table 3 are real and indicate true variations of deceleration from place to place around the occulting disk. The flows at S33°W and S85°W are notable examples. At S33°W the initial speed is ~800 km/s, falling to 300 km/s in 2.1 hours, corresponding to a deceleration of 67 m/s^2. By comparison, the speed at S85°W falls from 500 to 240 km/s in 4.6 hours, corresponding to 16 m/s^2. These trends are also apparent from a comparison of the corresponding height/time tracks in Figure 5b.

3. Summary and Discussion

In a previous study we measured the speeds and accelerations of a variety of coronal features, including the blobs of material that detach from streamers, the slow CMEs that seem to erupt from streamers, and the fast CMEs associated with impulsive solar events [*Sheeley et al*., 1999]. The streamer-related ejecta gradually accelerated to speeds in the range 300–400 km/s or more as they moved through the 30 R_S field of view, but the fast CMEs moved uniformly at speeds that were typically in excess of 700 km/s.

Decelerating motions were rare but could always be found in fast halo CMEs and along the flanks of fast CMEs seen from an oblique perspective (quasi-halo CMEs). It was puzzling that decelerating features seemed to avoid the sky plane and made us wonder if the deceleration occurred at radial distances beyond 30 R_S. If so, the observed decelerations of these super-Alfvenic events might be the result of shock waves sweeping up mass from the large volume of space available far from the Sun.

We have continued to study fast CMEs during 1998 and 1999 and have again found uniform speeds at the leading edges of these events and decelerations along their flanks and rear. However, in this new study we found that the decelerating features were often kinks traveling radially outward along coronal rays. These rays included not only bright streamers whose CME-induced deflections are similar to those observed with previous coronagraphs [*Gosling et al*., 1974; *Michels et al*., 1984; *Sime and Hundhausen*, 1987] but also very faint rays like those seen recently in LASCO images [*Wang et al*., 1998] and in ground-based eclipse images [*Guhathakurta and Fisher*, 1995]. Coronal intensity simulations [*Wang*, 1996] suggest that these rays may be small-scale spines in the thin plasma sheet that winds around the Sun and produces bright streamers when seen edge on.

With the advance of the sunspot cycle this plasma sheet has become increasingly distorted, and its rays are now visible in all directions around the Sun, providing a medium for detecting the global influence of fast CMEs. Thus, when a fast CME occurs, there are almost always distant streamers and rays to push. By contrast, near sunspot minimum, fast CMEs were rare, and when they did occur, the streamers were always at the equator in more or less the same place as the CMEs. As a result, the number of decelerating events for which we have made height/time maps increased from 8 in 1997 to 17 in 1998 to 42 in the first 10 months of 1999.

The wide range of position angles of these deflected rays makes it seem unlikely that all of them would lie out of the sky plane at large radial distances from the Sun and suggests that

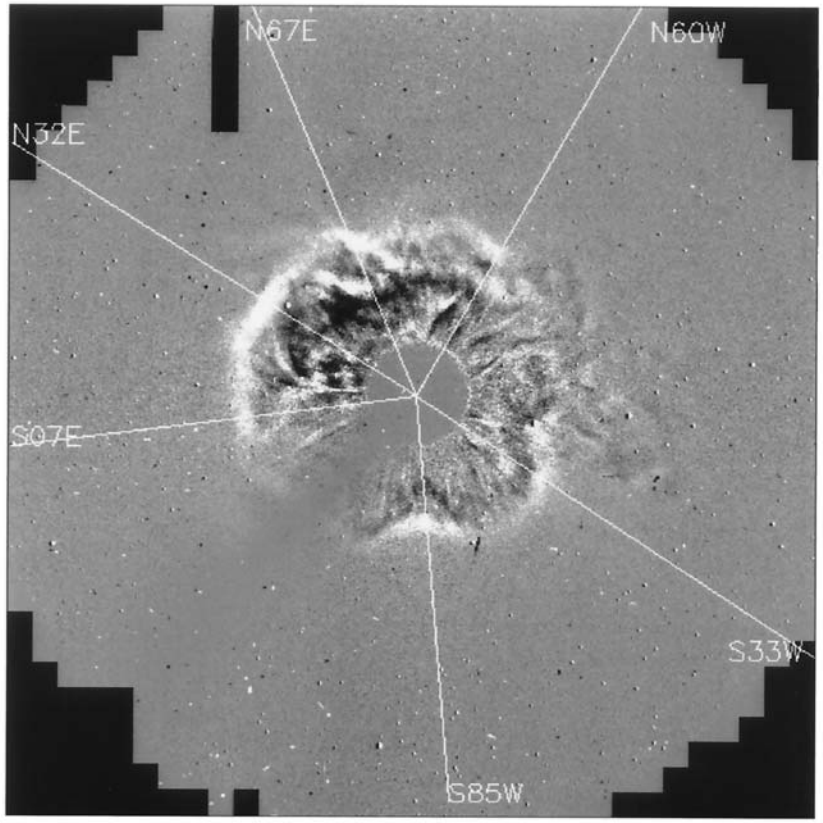

Figure 5a. A C3 difference image of the June 29, 1999, halo CME, showing the six paths around the occulting disk for which the height/time maps in Figure 5b were constructed. The full C3 field of view is shown, extending to 30 R_S in the horizontal and vertical directions and to 32 R_S in the corners.

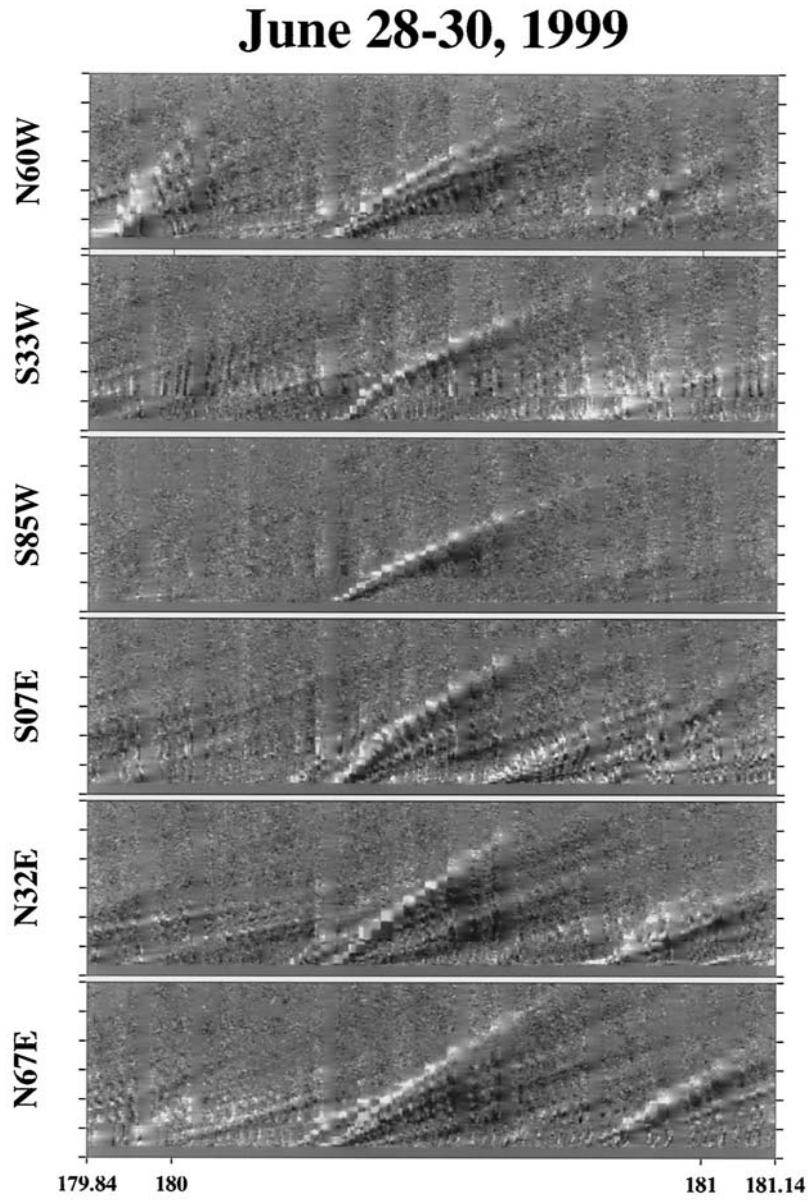

Figure 5b. Height/time maps for the six locations indicated in Figure 5a, showing downward curving profiles (i.e., decelerations) in all of these directions. The horizontal scale indicates time expressed as a day of year, and the vertical scale indicates elongation expressed in solar radii from 0 to 30 R_S.

we may need to find another explanation for the observed decelerations. One possibility is that the shock wave loses energy and slows down as it pushes obliquely across the radial magnetic field lines indicated by the deflected streamers and rays. This would account for the tendency of the deceleration to avoid the front of the CME where the field lines are nearly parallel to the propagation direction of the wave front. This explanation would also account for the decelerations of fast halo CMEs, like the July 29, 1999, event in Figures 4a and 5a. In this case, the observed outward motion would be interpreted as the sky plane projection of the shock front as it moves across the streamers and rays or, equivalently, as the sky plane projection of the radially moving kinks that the shock produces as it moves across those streamers and rays.

In this regard, it is interesting to recall that *St. Cyr and Hundhausen* [1987] suggested that some halo CMEs may consist of streamers that have been deflected away from the line of sight. We have seen such deflected rays along the sides and toward the rear of quasi-halo CMEs, like those on July 6 and July 25, 1999, in Figures 1a and 3a. Such deflections must contribute to the ragged spatial structure that distinguishes fast halo CMEs from gradually accelerating halo CMEs [*Sheeley et al*., 1999]. On the other hand, we doubt that the leading edges of fast halo CMEs consist entirely of deflected streamers. The leading edges of some quasi-halo CMEs, like the July 6, 1999, CME in Figures 3a and 3b, show deceleration, and it seems likely that they would also show deceleration when seen head-on (or tail-on).

We have assumed that the CME-associated waves are shock waves rather than compressive MHD waves because the initial speeds are of the order of 800–1400 km/s or more toward the fronts and sides of the CMEs where the sky plane corrections are small. Unknown projection effects make it difficult to determine the lateral speed of the wave front when the CME is seen broadside. However, we can obtain a reasonable estimate when the CME is aimed along the line of sight. For example, the initial speeds of the July 29, 1999, halo CME were in the range 500–800 km/s (see Table 3). These speeds are close enough to the nominal 600 km/s Alfven speed at 3 R_S [*Hundhausen*, 1999] to leave some doubt as to whether they are really super-Alfvenic. Of course, the case for super-Alfvenic flow becomes stronger when one allows for the fact that the halo lies out of the sky plane at a radial distance greater than 3 R_S, where the Alfven speed is lower than 600 km/s and may be as small as 400 km/s.

In contrast to the streamers and rays that are temporarily deflected by waves from distant, fast CMEs as described in this paper, we have also observed streamers that are gradually pushed aside by slow, accelerating outflows. These more permanent deflections do not decelerate but instead share the accelerating motions of the slow material that is pushing them.

It is interesting to consider why fast CME-associated shocks have not been seen previously. LASCO contains several improvements over previous coronagraphs, including the high spatial resolution of C2, the wide field of C3, and the improved sensitivity and data-handling capability of both instruments. However, the most significant improvement was to the dynamic range, which is about 50,000 compared to only 50–70 for the SOLWIND coronagraph. This improvement is probably responsible for our ability to see very faint "precursors" and deflected rays like those in Figures 1a–1b as well as the faint "blobs" of material that accelerate outward along streamers [*Sheeley et al*., 1997]. By comparison, the relatively low dynamic range of the SOLWIND coronagraph probably prevented us from seeing such features with that instrument [*Karpen and Howard*, 1987]. Finally, we should not underestimate the importance of the continuous height/time maps. They revealed the decelerations that seem to characterize these fast CME-associated disturbances.

Acknowledgments. LASCO is a multinational team effort by the Max-Planck-Institut für Aeronomie (Katlenburg-Lindau, Germany), the Laboratoire d'Astronomie Spatiale (Marseille, France), the University of Birmingham School of Physics and Astronomy (Birmingham, England), and the Naval Research Laboratory (Washington, D. C.). We are grateful to our LASCO colleagues for making this study possible. At NRL, N. B. Rich and D. Wang generously helped with the data processing and imaging software; R. A. Howard and O. C. St. Cyr provided encouragement and thoughtful discussions of coronal mass ejections; and D. J. Michels contributed helpful information and ideas about the LASCO instrument. We are also grateful to our colleagues at the Institut d'Astrophysique Spatiale (Orsay, France) for use of the complementary EIT images. Financial support for this study was provided by the Office of Naval Research/NRL Research Option "Solar Magnetism and Earth's Environment," and by NASA.

Janet G. Luhmann thanks Simon Plunkett and Rainer Schwenn for their assistance in evaluating this paper.

References

Bates, K. L., America the Beautiful, *Congregationalist*, July 4, 1895.

Bougeret, J.-L., Observations of shock formation and evolution in the solar atmosphere, in *Collisionless Shocks in the Heliosphere: Reviews of Current Research*, *Geophys. Monogr. Ser*., vol. 35, edited by B. T. Tsurutani and R. G. Stone, p. 13, AGU, Washington, D. C., 1985.

Cane, H. V., and R. G. Stone, Type II radio bursts, interplanetary shocks, and energetic particle events, *Astrophys. J*., *282*, 339, 1984.

Cane, H. V., R. G. Stone, J. L. Fainberg, and S. Hoang, Type II solar radio events observed in the interplanetary medium, *Sol. Phys*., *78*, 187, 1982.

Cane, H. V., N. R. Sheeley Jr., and R. A. Howard, Energetic interplanetary shocks, radio emission, and coronal mass ejections, *J. Geophys. Res*., *92*, 9869, 1987.

Gold, T., Discussion of shock waves and rarefied gases, in *Gas Dynamics of Cosmic Clouds*, *IAU Symp*., no. 2, edited by H. C. van de Hulst and J. M. Burgers, p. 103, North-Holland, New York, 1955.

Gosling, J. T., E. Hildner, R. M. MacQueen, R. H. Munro, A. I. Poland, and C. L. Ross, Mass ejections from the Sun: A view from Skylab, *J. Geophys. Res*., *79*, 4581, 1974.

Gosling, J. T., E. Hildner, R. M. MacQueen, R. H. Munro, A. I. Poland, and C. L. Ross, Direct observations of a flare-related coronal and solar wind disturbance, *Sol. Phys*., *40*, 439, 1975.

Guhathakurta, M., and R. R. Fisher, Coronal streamers and fine-scale structures of the low-latitude corona as detected with SPARTAN 201-01 white light coronagraph, *Geophys. Res. Lett*., *22*, 1841, 1995.

Hundhausen, A. J., The origin and propagation of coronal mass ejections, in *Proceedings of the 6th International Solar Wind Conference*, vol. I, edited by V. J. Pizzo, T. Holzer, and D. G. Sime, p. 181, High Altitude Obs., Natl. Cent. for Atmos. Res., Boulder, Colo., 1987.

Hundhausen, A. J., Coronal mass ejections: A summary of SMM observations from 1980 and 1984–1989, in *The Many Faces of the Sun; Scientific Highlights of the Solar Maximum Mission*, edited by K. T. Strong et al., p. 143, Springer-Verlag, New York, 1999.

Karpen, J. T., and R. A. Howard, A search for forerunner activity associated with coronal mass ejections, *J. Geophys. Res*., *92*, 7227, 1987.

Liepmann, H., Discussion of shock waves and rarefied gases, in *Gas Dynamics of Cosmic Clouds*, *IAU Symp*., no. 2, edited by H. C. van de Hulst and J. M. Burgers, p. 104, North-Holland, New York, 1955.

Michels, D. J., N. R. Sheeley Jr., R. A. Howard, M. J. Koomen, R. Schwenn, K. H. Mühlhäuser, and H. Rosenbauer, Synoptic observations of coronal transients and their interplanetary consequences, *Adv. Space Res*., *4*(7), 311, 1984.

Parker, E. N., *Interplanetary Dynamical Processes*, p. 93, John Wiley, New York, 1963.

Robinson, R. D., R. T. Stewart, N. R. Sheeley Jr., R. A. Howard, M. J. Koomen, and D. J. Michels, Properties of metre wavelength solar

bursts associated with coronal mass ejections, *Sol. Phys*., *105*, 149, 1986.

Schwenn, R., Relationship of coronal transients to interplanetary shocks, 3-d aspects, *Space Sci. Rev*., *44*, 139, 1986.

Sheeley, N. R., Jr., Using LASCO observations to infer solar wind speed near the Sun, in *Solar Wind Nine*, edited by S. R. Habbal et al., *AIP Conf. Proc*., *471*, 41, 1999.

Sheeley, N. R., Jr., R. T. Stewart, R. D. Robinson, R. A. Howard, M. J. Koomen, and D. J. Michels, Associations between coronal mass ejections and metric type II bursts, *Astrophys. J*., *279*, 839, 1984.

Sheeley, N. R., Jr., R. A. Howard, M. J. Koomen, D. J. Michels, R. Schwenn, K. H. Mühlhäuser, and H. J. Rosenbauer, Coronal mass ejections and interplanetary shocks, *J. Geophys. Res*., *90*, 163, 1985.

Sheeley, N. R., Jr., et al., Measurements of flow speeds in the corona between 2 and 30 R_S, *Astrophys. J*., *484*, 472, 1997.

Sheeley, N. R., Jr., J. H. Walters, Y.-M. Wang, and R. A. Howard, Continuous tracking of coronal outflows: Two kinds of coronal mass ejections, *J. Geophys. Res*., *104*, 24,739, 1999.

Sime, D. G., and A. J. Hundhausen, The coronal mass ejection of July 6, 1980: A candidate for interpretation as a coronal shock wave, *J. Geophys. Res*., *92*, 1049, 1987.

Sonett, C. P., D. S. Colburn, L. Davis, and P. J. Coleman Jr., Evidence for a collision-free hydromagnetic shock wave in interplanetary space, *Phys. Rev. Lett*., *13*, 153, 1964.

St. Cyr, O. C., and A. J. Hundhausen, On the interpretation of "Halo" coronal mass ejections, in *Proceedings of the 6th International Solar Wind Conference*, vol. I, edited by V. J. Pizzo, T. Holzer, and D. G. Sime, p. 235, High Altitude Obs., Natl. Cent. for Atmos. Res., Boulder, Colo., 1987.

Steinholfson, R. S., Theories of shock formation in the solar atmosphere, in *Collisionless Shocks in the Heliosphere: Reviews of Current Research*, *Geophys. Monogr. Ser*., vol. 35, edited by B. T. Tsurutani and R. G. Stone, p. 1, AGU, Washington, D. C., 1985.

Wagner, W. J., and R. M. MacQueen, The excitation of type II radio bursts in the corona, *Astron. Astrophys*., *120*, 136, 1983.

Wang, Y.-M., Non-radial coronal streamers, *Astrophys. J*., *456*, L119, 1996.

Wang, Y.-M., et al., Origin and evolution of coronal streamer structure during the 1996 minimum activity phase, *Astrophys. J*., *485*, 875, 1998.

Wild, J. P., and S. F. Smerd, Radio bursts from the solar corona, *Annu. Rev. Astron. Astrophys*., *10*, 159, 1972.

Wild, J. P., J. D. Murray, and W. C. Rowe, Evidence of harmonics in the spectrum of a solar radio outburst, *Nature*, *172*, 533, 1953.

Wild, J. P., S. F. Smerd, and A. A. Weiss, Solar bursts, *Annu. Rev. Astron. Astrophys*., *1*, 291, 1963.

W. N. Hakala, Asian and Middle Eastern Languages, Cabell Hall, University of Virginia, Charlottesville, VA 22903.

N. R. Sheeley Jr. and Y.-M. Wang, E. O. Hulburt Center for Space Research, Naval Research Laboratory, Code 7672W, 4555 Overlook Ave., S. W., Washington, DC 20375-5352. (sheeley@spruce.nrl.navy.mil)

(Received September 15, 1999; revised December 2, 1999; accepted December 2, 1999.)